

A Multisite Decomposition of the Tensor Network Path Integrals

Amartya Bose*

Department of Chemistry, Princeton University, Princeton, New Jersey 08544

Peter L. Walters*

*Department of Chemistry, University of California, Berkeley, California 94720 and
Miller Institute for Basic Research in Science, University of California Berkeley, Berkeley, California 94720*

Recently tensor network decompositions of path integrals for simulation of open systems have proven to be useful. In this work, we extend the tensor network path integral (TNPI) framework to efficiently simulate extended systems coupled with local vibrational and phononic modes. This multisite decomposition of TNPI (MS-TNPI) combines a matrix product state decomposition of the reduced density tensor of the system along the sites with a corresponding tensor network representation of the time axis to construct an efficient 2D tensor network. This 2D MS-TNPI network can be systematically contracted to yield the time-dependent reduced density tensor of the system. The decomposition and algorithm presented is independent of the nature of the system Hamiltonian. We also outline an iteration scheme to take the simulation beyond the non-Markovian memory length. Applications to spin chains coupled to a harmonic bath is presented; we consider interactions defined by the Ising, XXZ and the Heisenberg models. The MS-TNPI method would be useful for studying a variety of extended quantum systems coupled with a vibrational baths or phononic modes.

I. INTRODUCTION

Quantum effects in dynamics are often very important for studying charge or exciton energy transfer in long chains and in understanding decoherence in systems of qubits. To curtail the exponential growth of computational complexity, a system-solvent description is often used. While in many cases it is indeed possible to limit the quantum description to only a small subspace of degrees of freedom, for extended systems, this quantum subspace or “system” can be quite large in and of itself. Thus, the effectiveness of a typical system-solvent decomposition might be questioned. Methods like density matrix renormalization group [1–4] (DMRG) and its time-dependent variant [5–7] (tDMRG) are very useful in simulating these large systems by decomposing the wave function along the “system” axis using sequential singular value decompositions (SVD). Multiconfiguration time-dependent Hartree (MCTDH) and its multi-level version (ML-MCTDH) constitute another family of tensor network-based algorithms that have also been commonly used to simulate non-equilibrium dynamics. However, when vibrational or phononic modes are present, the wave function-based nature of these algorithms pose significant computational challenges. Also, a proper description of thermal equilibrium is not truly possible using a wave function-based method [8].

Path integrals provide a lucrative alternative for simulating open quantum systems. Feynman-Vernon influence functional (IF) [9] and the hierarchical equations of motion (HEOM) [10] are rigorous methods for incorporating the interactions between systems and solvents without having to simulate the vibrational manifold ex-

plicitly. While HEOM is, in principle, exact for systems interacting with arbitrary harmonic baths, practically, it has been mostly restricted to simulating the case of a bath described by a Drude spectral density. Attempts have been made to develop efficient HEOM-based algorithms that are applicable to general spectral densities [8, 10–13]. In case the solvent is atomistically defined and anharmonic effects are important, the IF does not have a closed-form expression. Classical trajectories are often used for estimating the influence functional in such cases [14–18]. The quasi-adiabatic propagator path integrals (QuAPI) [19, 20] and related methods [21–23] are useful when simulating systems bilinearly coupled to a harmonic bath. Recently tensor networks have been shown to be efficient in making calculations with influence functionals more efficient [24–29].

Simulating thermal dynamics of extended systems coupled to a vibrational manifold poses unique challenges. As mentioned before, even though there have been attempts to incorporate the bath in terms of a basis set [30], wave function-based methods like DMRG or tDMRG are typically not well-suited. The computational complexity tends to grow because of the entanglement between the system states and the bath modes. Recently path integral based methods have been developed to account for extended system with short-ranged interactions as well [31–34]. Based on tensor network decompositions, Lerose *et al.* [35] have developed a method for simulating influence functionals for cases where the system and the environment are made of indistinguishable particles. In particular, they applied their method to calculate the reduced density matrix for a specific site in a spin-chain.

Tensor network path integrals (TNPI) [28] offer an approach to influence functional-based path integral simulations that can quite simply be extended to the problem of extended systems interacting with localized solvents. TNPI typically involves a matrix product state (MPS)

* Both authors contributed equally to this work.

representation of the “augmented propagator” (AP). In this paper, the MPS structure is extended to a novel two-dimensional structure that accounts for multiple system states leading to a multisite version of the TNPI framework (MS-TNPI). This MS-TNPI tensor network can be efficiently contracted and used to simulate the reduced density tensor of a quantum system composed of multiple sites. From a different perspective, MS-TNPI could be thought of as an extension of tDMRG to incorporate Feynman-Vernon influence functionals to account for interactions of sites with local solvents.

The MS-TNPI method allows for incorporation of longer-ranged interactions without any change to the fundamental structure of the problem, which is completely accounted for by the system propagator [4, 6]. The time-evolved reduced density tensor corresponding to the entire extended system is directly evaluated and represented in the form of an MPS. The method is implemented using the open-source ITensor library [36]. In Sec. II, we develop the structure of MS-TNPI. The method is illustrated with some examples in Sec. III. Finally, we end the paper with some concluding remarks and future prospects in Sec. IV.

II. METHODOLOGY

Consider a system consisting of P particles or sites each with its local vibrational degrees of freedom:

$$\hat{H} = \hat{H}_0 + \sum_{j=1}^P \hat{V}_j \quad (1)$$

where \hat{H}_0 is the system Hamiltonian and \hat{V}_j is the Hamiltonian encoding the system-vibration interaction localized on the j^{th} site.

Typically, the site-vibration interaction would have anharmonic terms, but under Gaussian response theory, the effect of the anharmonic vibrations can be accounted for by an equivalent harmonic bath on the j^{th} site:

$$\hat{V}_j = \sum_{l=1}^N \frac{p_{j,l}^2}{2m_{j,l}} + \frac{1}{2} m_{j,l} \omega_{j,l}^2 \left(x_{j,l} - \frac{c_{j,l} \hat{s}_j}{m_{j,l} \omega_{j,l}^2} \right)^2 \quad (2)$$

where $\omega_{j,l}$ and $c_{j,l}$ are the frequency and coupling of the l^{th} mode of the j^{th} site, and \hat{s}_j is the system operator corresponding to the j^{th} site that couples with the vibrations. The site-vibration interaction is characterized by a spectral density [37, 38]:

$$J(\omega) = \frac{\pi}{2} \sum_k \frac{c_k^2}{m_k \omega_k} \delta(\omega - \omega_k). \quad (3)$$

In case the vibrations are defined by atomistic Hamiltonians, it is often possible to obtain the spectral density as a Fourier transform of the energy-gap autocorrelation function obtained via classical trajectory simulations. In

case of interactions with phonons, typically the modes can be exactly described by harmonic oscillators even without invoking Gaussian response theory.

The dynamics of a system coupled to a harmonic bath is well-described by the formalism of Feynman-Vernon influence functionals (IF). This starts with a computation of the forward-backward propagator of the bare system, which is defined as the direct product of the forward and backward propagators for a short time-step. Typically, they are calculated using the Suzuki-Trotter decomposition. Let $K(S_0^\pm, S_1^\pm, \Delta t)$ be the forward-backward propagator connecting the system defined by S_0^\pm at the initial time point and S_1^\pm at the final time point. The notation S_k^\pm represents the state of all the sites at the k^{th} time point, where the j^{th} site is denoted by $s_{j,k}^\pm$. The presence of the bath brings in non-Markovian effects and prevents an iterative propagation of the reduced density tensor of the extended system. Incorporating the IF leads to the following equations [19, 20]:

$$\begin{aligned} \tilde{\rho}(S_N^\pm, N\Delta t) &= \text{Tr}_{\text{bath}} \langle S_N^+ | \rho(N\Delta t) | S_N^- \rangle \\ &= \sum_{S_0^\pm} \tilde{\rho}(S_0^\pm, 0) G(S_0^\pm, S_N^\pm, N\Delta t) \end{aligned} \quad (4)$$

$$G(S_0^\pm, S_N^\pm, N\Delta t) = \sum_{S_1^\pm} \cdots \sum_{S_{N-1}^\pm} P_{S_0^\pm \cdots S_N^\pm} \quad (5)$$

$$= \sum_{S_1^\pm} \cdots \sum_{S_{N-1}^\pm} F[\{S_k^\pm\}] P_{S_0^\pm \cdots S_N^\pm}^{(0)} \quad (6)$$

where

$$P_{S_0^\pm \cdots S_N^\pm}^{(0)} = K(S_0^\pm, S_1^\pm, \Delta t) \times \cdots \times K(S_{N-1}^\pm, S_N^\pm, \Delta t) \quad (7)$$

is the bare path amplitude tensor and $F[\{S_k^\pm\}]$ is the influence functional for the particular forward-backward system path in question. The path amplitude tensor, $P_{S_0^\pm \cdots S_N^\pm}$, which appears in Eq. (6), has $O(d^{2NP})$ coefficients, where d is the dimensionality of a typical system site, N is the number of time points and P is the number of sites. The number of coefficients grows exponentially with both the number of sites as well as the number of time points. In this work, we aim to combat this exponential growth, by factorizing this unmanageably large tensor into a 2D network of smaller ones.

We start by representing the forward-backward propagator, K , in the form of a matrix product operator (MPO).

$$K(S_0^\pm, S_1^\pm, \Delta t) = \sum_{\{\alpha_j\}} W_{\alpha_1}^{s_{10}^\pm, s_{11}^\pm} W_{\alpha_1, \alpha_2}^{s_{20}^\pm, s_{21}^\pm} \cdots W_{\alpha_{P-1}}^{s_{P0}^\pm, s_{P1}^\pm}. \quad (8)$$

Here, a typical “site” index, s_{ij}^\pm has two subscripts: the first subscript of s_{ij}^\pm , i , is for the site (or particle) number and the second one, j , indicates the time point. In principle any forward-backward propagator can be represented

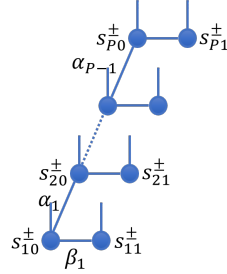


FIG. 1. Factorization of the forward-backward MPO following Eqs. (9)–(11)

as a MPO, but doing so may be as costly as directly solving the Schrödinger equation. Fortunately, using matrix product representations for studying dynamics of the bare system has been a topic of intense research over the years. Various methods like time-dependent variational principle (TDVP) [39–41], time-evolving block decimation (TEBD) [5, 42, 43] and time-dependent DMRG (tDMRG) [5, 7] have been developed to directly simulate the time evolution of such extended systems. For systems with long-ranged interactions, the recently introduced MPO $W^{I,II}$ method [44] can generate very efficient representations of the propagator. While TEBD and MPO $W^{I,II}$ calculate the propagators, Krylov subspace-based methods and TDVP often approximate the action of the propagator on the wave function. Detailed comparisons of these methods for the purposes of simulating the propagator, especially in the context of the current method, is extremely interesting and beyond the scope of this paper. A thorough study of these ideas would be conducted in the future. For the current development, we will simply assume that a MPO representation of the forward-backward propagator is available.

The effect of dissipative environments is handled by Feynman-Vernon influence functional (IF) [9] and involves a non-Markovian memory term. In order to incorporate it in a tensor network formalism, it is convenient to represent the path tensor as a matrix product structure with the different time points as its sites [24, 25, 27, 28]. In this spirit, we proceed by decomposing the forward-backward propagator further in the following manner:

$$W_{\alpha_1}^{s_{10}^{\pm}, s_{11}^{\pm}} = \sum_{\beta_{11}} L_{\alpha_1, \beta_{11}}^{s_{10}^{\pm}} R_{\beta_{11}}^{s_{11}^{\pm}} \quad (9)$$

$$W_{\alpha_{j-1}, \alpha_j}^{s_{j0}^{\pm}, s_{j1}^{\pm}} = \sum_{\beta_{j1}} L_{\alpha_{j-1}, \alpha_j, \beta_{21}}^{s_{j0}^{\pm}} R_{\beta_{21}}^{s_{j1}^{\pm}}, \quad 1 < j < P \quad (10)$$

$$W_{\alpha_{P-1}}^{s_{P0}^{\pm}, s_{P1}^{\pm}} = \sum_{\beta_{P1}} L_{\alpha_{P-1}, \beta_{P1}}^{s_{P0}^{\pm}} R_{\beta_{P1}}^{s_{P1}^{\pm}}. \quad (11)$$

The bonds along the “spatial” dimension are denoted by α , and β represents the bonds along the “temporal” dimension. Figure 1 shows this structure in the form of a tensor diagram.

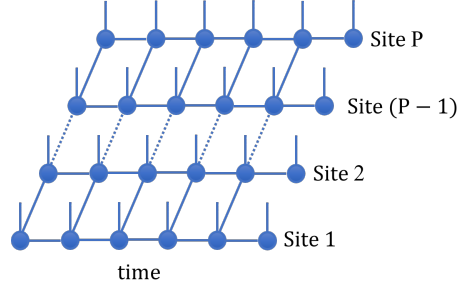


FIG. 2. Factorization of the forward-backward MPO.

For the next time step, we extend the structure in a systematic manner. The intermediate tensors would have an augmented structure. Consider the tensors at an intermediate time point, n :

$$M_{\alpha_{(1,n)}, \beta_{(1,n+1)}, \beta_{(1,n)}}^{s_{1,n}^{\pm}} = R_{\beta_{1,n}}^{s_{1,n}^{\pm}} L_{\alpha_{(1,n)}, \beta_{(1,n+1)}}^{s_{1,n}^{\pm}} \quad (12)$$

$$M_{\alpha_{(j,n)}, \beta_{(j,n+1)}, \alpha_{(j-1,n)}, \beta_{(j,n)}}^{s_{j,n}^{\pm}} = R_{\beta_{j,n}}^{s_{j,n}^{\pm}} L_{\alpha_{(j-1,n)}, \alpha_{(j,n)}, \beta_{(j,n+1)}}^{s_{j,n}^{\pm}} \quad (13)$$

$$M_{\beta_{(P,n+1)}, \alpha_{(P-1,n)}, \beta_{(P,n)}}^{s_{P,n}^{\pm}} = R_{\beta_{P,n}}^{s_{P,n}^{\pm}} L_{\alpha_{(P-1,n)}, \beta_{(P,n+1)}}^{s_{P,n}^{\pm}}. \quad (14)$$

Please note that the parentheses on the “coordinates” of the bond indices, α and β , have been used only for visual clarity. Their absence or presence do not change the meaning of the equation. The tensors on the initial time point won’t have the contributions from R tensors. They are defined as follows:

$$M_{\alpha_{(1,0)}, \beta_{(1,1)}}^{s_{1,0}^{\pm}} = L_{\alpha_{(1,0)}, \beta_{(1,1)}}^{s_{1,0}^{\pm}} \quad (15)$$

$$M_{\alpha_{(j,0)}, \beta_{(j,1)}, \alpha_{(j-1,1)}}^{s_{j,0}^{\pm}} = L_{\alpha_{(j-1,0)}, \alpha_{(j,1)}, \beta_{(j,1)}}^{s_{j,0}^{\pm}} \quad (16)$$

$$M_{\alpha_{(P-1,0)}, \beta_{(P,1)}}^{s_{P,0}^{\pm}} = L_{\alpha_{(P-1,0)}, \beta_{(P,1)}}^{s_{P,0}^{\pm}}. \quad (17)$$

At the final time point, N , the tensors lack contributions from the L tensors and are given by:

$$M_{\beta_{(1,N)}}^{s_{1,N}^{\pm}} = R_{\beta_{1,N}}^{s_{1,N}^{\pm}} \quad (18)$$

$$M_{\beta_{(j,N)}}^{s_{j,N}^{\pm}} = R_{\beta_{j,N}}^{s_{j,N}^{\pm}} \quad (19)$$

$$M_{\beta_{(P,N)}}^{s_{P,N}^{\pm}} = R_{\beta_{P,N}}^{s_{P,N}^{\pm}}. \quad (20)$$

Putting these M tensors together, we get the 2D structure illustrated in Fig. 2. Notice that here as well, the sites on the final time point are not connected together, Eqs. (18)–(20), inheriting the fundamental asymmetry between the initial and final time points in the structure in Fig. 1. This structure in case of a bare system is simply a further factorization of the simulation done much more efficiently by the Markovian propagation using tDMRG, TEBD or TDVP.

The flexibility of this factorization becomes apparent when the bath interactions in form of an IF is incorporated. The 2D structure discussed till now can be thought of as a series of generalized tensor networks along the “columns” that represent the state of the full system at a given time point, or along the “rows” that represent the state of one site at all times or the AP of that particular site. While thinking of it as a collection of columns manifestly links the method to its tDMRG heritage, its identification as a collection of “row” tensors serve to illustrate how this multisite method is related to AP-TNPI [28]. If there was no interaction between the systems, the rows would separate out and every site would behave like the standard AP method. This makes it quite simple to take the influence functional into account.

For the case of site-local baths, the full IF would just be a product of the IFs on each of the sites. Since the structure of the IF is the same irrespective of the site, consider the p^{th} site. If the path of the site is given by $\{s_{p,j}^{\pm}\}$, then the IF [9] is:

$$F[\{s_{p,j}^{\pm}\}] = \exp \left(-\frac{1}{\hbar} \sum_{0 \leq k \leq N} \Delta s_{p,k} \sum_{0 \leq k' \leq k} (\text{Re}(\eta_{kk'}) \Delta s_{p,k'} \right. \\ \left. + 2i \text{Im}(\eta_{kk'}) \bar{s}_{p,k'}) \right) \quad (21)$$

where $\Delta s_{p,k} = s_{p,k}^+ - s_{p,k}^-$ and $\bar{s}_{p,k} = \frac{s_{p,k}^+ + s_{p,k}^-}{2}$ and $\eta_{kk'}$ are the discretized η -coefficients [19, 20]. It is possible to have different baths associated with different sites leading to a site-dependent η -coefficient and site-dependent influence functional, however for notational convenience, we describe the method assuming the baths on different sites are characterized by the same spectral density.

We have already discussed the analytical form for the matrix product operator for the IF [28]. Following that procedure, Eq. (21) is factorized based on the k time point:

$$F_k[\{s_{p,j}^{\pm}\}] = \exp \left(-\frac{1}{\hbar} \Delta s_{p,k} \sum_{0 \leq k' \leq k} (\text{Re}(\eta_{kk'}) \Delta s_{p,k'} \right. \\ \left. + 2i \text{Im}(\eta_{kk'}) \bar{s}_{p,k'}) \right) \quad (22)$$

and each F_k is given an MPO-representation, \mathbb{F}_k . The MPOs are applied to each row of the 2D multisite TNPI structure for each system site in order of increasing k as detailed in Ref. [28].

After application of the influence functional MPO, the tensor network, Fig. 2, is contracted. This contraction can be done in two ways: (1) if the Green’s function for the propagation is required, we contract only the intermediate site indices to obtain an MPO; (2) if we want the

reduced density tensor of the system, we first contract the initial point with the initial density tensor directly, followed by tracing over all the intermediate time points. Of course, method (2) is computationally more efficient and sufficient for most simulations. For this step, consider the network, Fig. 2, as a sequence of columns, each representing the state of the system at a given time point. The site indices at the intermediate time points need to be traced over, turning the corresponding columns into MPOs. The initial column becomes an MPS. This is schematically demonstrated in Fig. 3. The sequence of applications of MPO to MPS accounts for all the tensor operations except for the last column which consists of independent tensors being applied to each site. This results in an MPS representation of the reduced density tensor corresponding to the system.

It is well-known that for simulations in the condensed phase, the non-Markovian memory does not extend for all of history. This means that the paths can be truncated after L time steps, to simulate a non-Markovian memory of time-span $L\Delta t$. To develop such an iteration procedure, one needs to know the full state of the system at any time point. We have access to that information for the extended system in the form of the corresponding column in the 2D lattice structure, Fig. 2. Iteration can also be done in two ways — for the Green’s function as done in Ref. [28], or as typically done, for a particular initial state [19, 20]. Once again in the interest of simplicity of discussion and computational efficiency, we describe the iteration scheme for a particular initial reduced density tensor. For a simulation with memory length L , consider the steps for simulating the first time point beyond memory, $t = (L + 1)\Delta t$:

1. Apply the MPO formed by the first column of multisite 2D tensor network, C_1 , to the initial reduced density tensor MPS and subsequently, multiply by the second column, C_2 to give rise to an MPO, \tilde{C}_1 . This MPO will serve as the first column of the iterated 2D structure.
2. The j^{th} column of the iterated 2D structure would be the same as the $(j + 1)^{\text{th}}$ column of the old 2D network. This allows us to fill the first L of the $L + 1$ columns.
3. The final column is the final time column, and is filled according to Eqs. (18)–(20).
4. The influence functional MPO corresponding to the last point is applied.

Subsequently, the steps of iteration happen in the similar manner. The only exception is step 1. Instead of applying the first column C_1 of the old network to the initial reduced density MPS, the site index is traced over. Figure 3 also highlights this difference between a time-step within the full-memory regime and in the iterative regime using the red marker MPS.

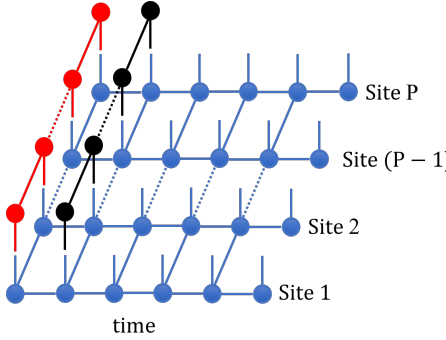


FIG. 3. Contraction of multisite tensor network. The red MPS would be the initial density tensor when simulating within memory, and it would be just the identity tensors when iterating. The black MPS represents the sequence of identity tensors that need to be applied to an intermediate time point to trace over them.

Finally, given the immense difficulty of the problem at hand, it is of interest to estimate the complexity of the algorithm outlined. The two most computationally demanding operations that occur during each time step are the application of the IF MPO and the contraction of the resulting tensor network. Roughly speaking, the cost of applying the IF MPO is $O(m_t^3 w_p^2 w_I^2 d^2 LP)$ and cost of the contraction is $O(m_s^3 w_p^2 m_t LP)$. Here, m_t is the typical bond dimension along the time axes (i.e., a row), m_s is the typical bond dimension along the system axes (i.e., a column), w_I is the typical bond dimension of the IF MPO. The typical bond dimension of the forward-backward propagator of the bare system is denoted by w_p , d is the dimensionality of a typical system site and P is the number of system sites. L is the non-Markovian memory length. It is clear from the scaling that both the terms are linear in L and P . Though the magnitude of m_t might be dependent on the memory length, L , the exponential growth of complexity within memory is effectively curtailed [28]. Since the local vibrational baths would typically consist of high frequency modes (implying that the non-Markovian memory length, L , is not very large), and the site-site couplings would be quite high, the cost would probably be dominated by the contraction process. However, if the local baths are very strongly coupled, the temporal bond dimension would grow much faster than the bond dimension along the system axis, and the pattern would be reversed.

III. RESULTS

For the purposes of illustrating the multisite TNPI method, we consider spin chains with nearest-neighbor intersite coupling.

$$\hat{H}_0 = \sum_{j=1}^P \hat{h}_j^{(1)} + \sum_{j=1}^{P-1} \hat{h}_{j,j+1}^{(2)} \quad (23)$$

where

$$\hat{h}_j^{(1)} = \epsilon \hat{\sigma}_z^{(j)} - \hbar \Omega \hat{\sigma}_x^{(j)} \quad (24)$$

is the one-body term and the two-body interaction term is given by a general nearest-neighbor Hamiltonian:

$$\hat{h}_{j,l}^{(2)} = \delta_{l,j+1} \left(J_x \hat{\sigma}_x^{(j)} \hat{\sigma}_x^{(l)} + J_y \hat{\sigma}_y^{(j)} \hat{\sigma}_y^{(l)} + J_z \hat{\sigma}_z^{(j)} \hat{\sigma}_z^{(l)} \right). \quad (25)$$

Here, $\hat{\sigma}_x^{(j)}, \hat{\sigma}_y^{(j)}, \hat{\sigma}_z^{(j)}$ are the Pauli spin matrices on the j^{th} site. Each of the sites is also coupled with its vibrational degrees of freedom described by the harmonic bath given in Eq. (2). For simplicity the harmonic bath is characterized by an Ohmic spectral density with an exponential decay:

$$J(\omega) = \frac{\pi}{2} \hbar \xi \omega \exp \left(-\frac{\omega}{\omega_c} \right) \quad (26)$$

where ξ is the dimensionless Kondo parameter, and ω_c is the characteristic cutoff frequency. In Appendix A, we outline the second-order Suzuki-Trotter splitting TEBD scheme used here to construct the forward-backward propagator MPO.

Depending on the nature of the intersite coupling, the models can be classified as an Ising model, a XXZ model or as the most general Heisenberg model. We provide illustrative examples of the dynamics in each case. The states of each system site are going to be called $|+1\rangle$ and $| -1\rangle$ which are eigenstates of the $\hat{\sigma}_z$ operator with eigenvalue of +1 and -1 respectively. In the following sections, the system consists of $P = 31$ sites. The bond dimension of the uncompressed forward-backward propagator MPO alternates between 16 for the odd bonds and 256 for the even bonds. Therefore, the average bond dimension for $P = 31$ sites is 136.

A. Ising Model

We first consider a transverse-field Ising model coupled with local vibrations. The system Hamiltonian is defined by the following one- and two- body terms:

$$\hat{h}_j^{(1)} = \epsilon \hat{\sigma}_z^{(j)} - \hbar \Omega \hat{\sigma}_x^{(j)} \quad (27)$$

$$\hat{h}_{j,l}^{(2)} = \delta_{l,j+1} J_z \hat{\sigma}_z^{(j)} \hat{\sigma}_z^{(l)} \quad (28)$$

where ϵ is the local asymmetry caused by an external longitudinal field, $\hbar \Omega$ is the strength of the transverse field, and J_z is the coupling between adjacent spin sites.

For the following examples, the one-body Hamiltonian defined by $\epsilon = 0$ and $\Omega = 1$. The dynamics is simulated for different values of the intersite coupling, $J_z = \pm 0.2, \pm 0.4, \pm 0.8$ and ± 1.6 . Initially, all the sites are localized at $|+1\rangle$. Here the bath is characterized by $\xi = 0.25$, $\omega_c = 5\Omega$, and it is held at an inverse temperature of $\hbar \beta \Omega = 1$. Figure 4 shows $\langle \hat{\sigma}_z(t) \rangle$ for the 16th spin

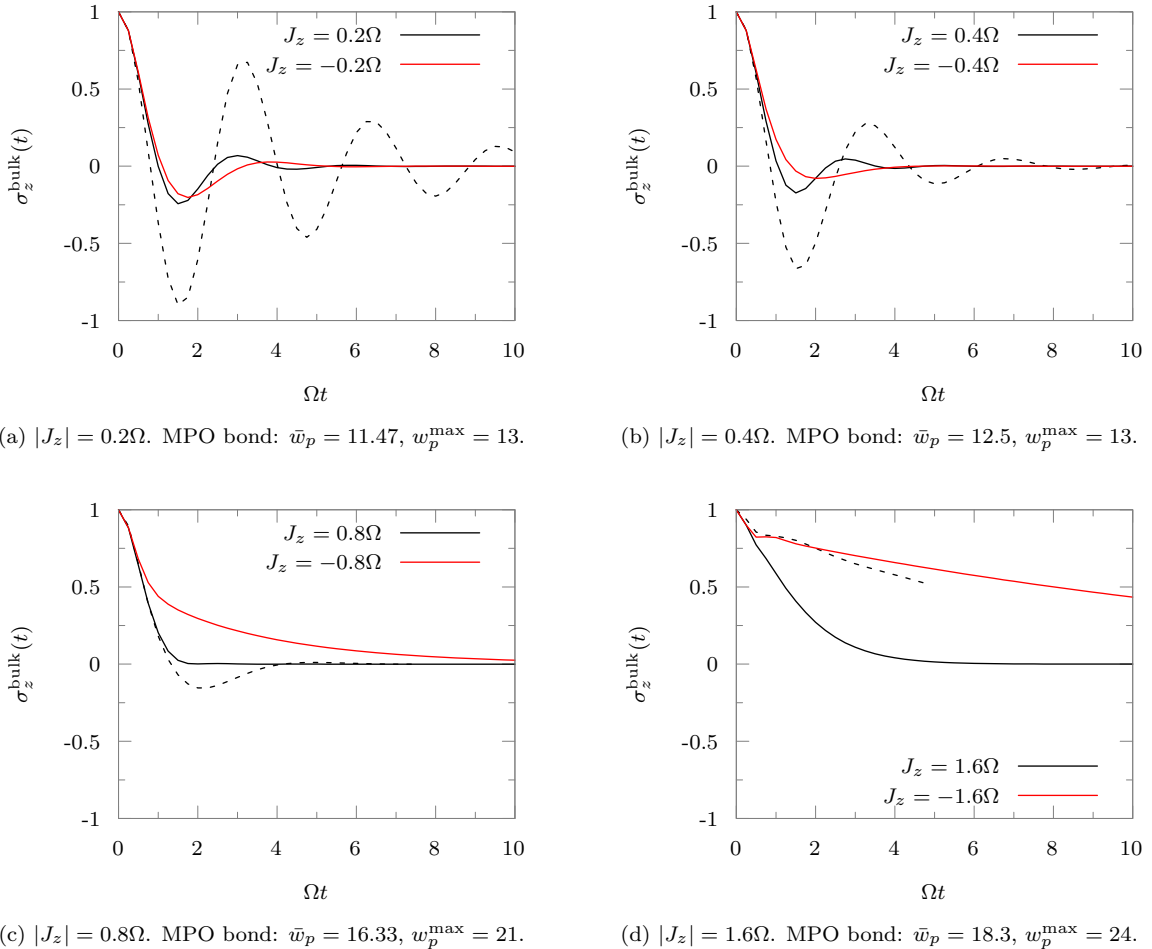


FIG. 4. Dynamics of a spin in the bulk as represented by $\langle \hat{\sigma}_z(t) \rangle$ for the 16th site of the Ising model coupled to an Ohmic bath. Dashed line: without bath.

in the chain. We observed that the finite size effects of the chain were limited only to a few edge sites and the dynamics of this middle monomer remained unaffected within the time-span of simulation, implying that this is the bulk dynamics.

A timestep of $\Delta t = 0.25$ was used. When the bath was present, a memory length of $L = 4$ was used, though acceptable convergence was already achieved at $L = 3$. The propagator was compressed using singular value decompositions with a cutoff of 10^{-11} . The average bond dimension (\bar{w}_p) and the maximum bond dimension (w_p^{max}) of the resultant compressed forward-backward propagator MPOs are listed in the captions of the figures. The dynamics of the bare system is shown for the various cases in dashed lines. It, unlike the dynamics in presence of the dissipative bath, remains the same irrespective of the sign of J_z . For the bare dynamics, we could use the MS-TNPI method and it would reduce to a density matrix version of TEBD. However, for efficiency, we propagated the wave function using TEBD.

The case of $J_z = -0.2\Omega$ (Fig. 4 (a) red line) was dis-

cussed by Makri [45] for a system with 10 sites. We recover identical bulk dynamics with our method. We are also able to span a very wide range of parameters as shown with very modest computational resources. We observe that the finite size of the chain affects more sites when J_z is larger. This is because for larger values of J_z , the sites “know” more about their neighbors, making the difference between an edge site with only one neighbor and a middle site with two neighbors more obvious.

B. XXZ Model

Another common model is the so-called XXZ-model of interactions between spins, where the two-body interaction term is defined by $J_x = J_y = J \neq 0$. In absence of any external field, the ratio between J_z and J is an order parameter for quantum phase transitions at zero temperature [46]. When $J_z < -J$, the ground state is ferromagnetic. There is a disordered spin-liquid phase when $-1 < \frac{J_z}{J} < 1$, and finally for $J_z > J$, there is an

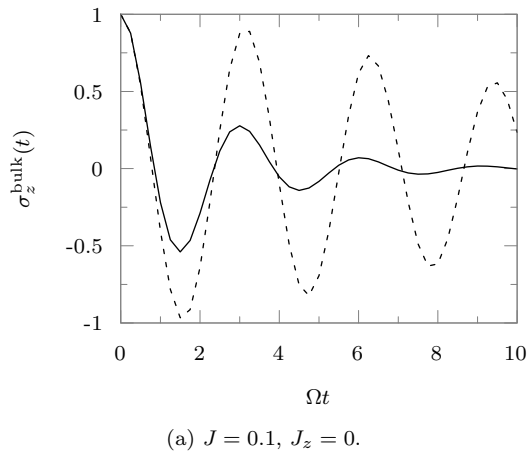
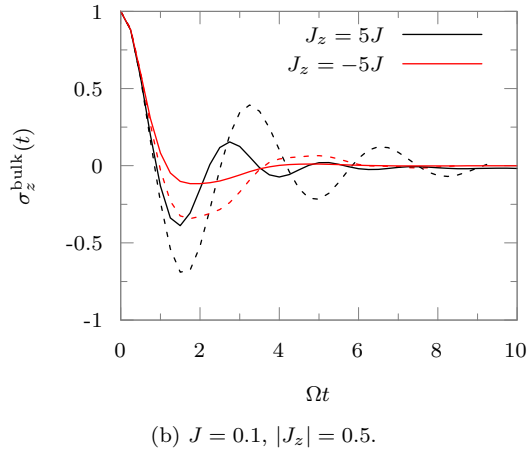
(a) $J = 0.1, J_z = 0$.(b) $J = 0.1, |J_z| = 0.5$.

FIG. 5. Dynamics of a spin in the bulk as represented by $\langle \hat{\sigma}_z(t) \rangle$ for the 16th site of the XXZ-model coupled to a harmonic bath. Dashed line: without bath.

antiferromagnetic state.

Here, we consider an XXZ system in an external transverse field of strength $\Omega = 1$ and with a longitudinal field of $\epsilon = 0$. The harmonic bath is once again held at an inverse temperature of $\hbar\Omega\beta = 1$. However in these examples it is characterized by $\xi = 0.2$, $\omega_c = 2$. We consider cases where $J_z = \pm 5J$ and $J_z = 0$. The time-step used for the convergence is $\Delta t = 0.25$. The dynamics of $\langle \hat{\sigma}_z(t) \rangle$ for a bulk spin, when the initial state defined by every spin in the $|+1\rangle$ state, is demonstrated for $J = 0.1$ and $J_x = 0, \pm 0.5$ in Fig. 5.

The compression of the propagator was done at a cutoff of 10^{-11} . For the case of $J_x = 0.5$, the maximum bond dimension for the compressed forward-backward propagator MPO is $w_p^{\max} = 68$ and the average bond dimension is $\bar{w}_p = 40.27$. When $J_z = -0.5$, $w_p^{\max} = 62$ and $\bar{w}_p = 37.47$. This slight difference in the bond dimensions stems from the actual compression that can be achieved. We note that the dynamics corresponding to the different values of J_z are totally different. It seems that the dissipation effects increase as the absolute value of J_z in-

creases. However, this increase in dissipation does not happen symmetrically. The effects coming from a negative J_z is much more pronounced than that caused by a positive value. These differences and the full effects of vibrational baths are very interesting and deserve a full analysis, that will be the subject of future work.

C. Heisenberg Model

The most general model for interacting spin chains is the so-called “Heisenberg” model. The Hamiltonian is characterized by a two-body spin-spin interaction term that involves couplings along X , Y and Z . Equations (24) and (25) describe a Heisenberg Hamiltonian in the most general case, when arbitrary and unconstrained values are used for J_x , J_y and J_z . The dynamics is started with all the spins localized on the $|+1\rangle$ state. The bath used for this example is the same as the one used for the XXZ-model examples.

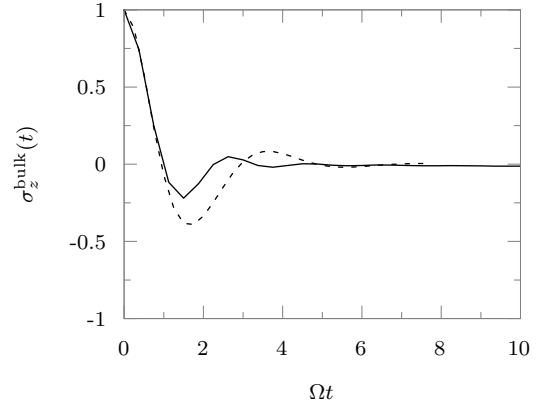


FIG. 6. Dynamics of a spin in the bulk represented by $\langle \hat{\sigma}_z(t) \rangle$ for the 16th site of the Heisenberg model coupled to a harmonic bath. Dashed line: without bath.

The dynamics of $\langle \hat{\sigma}_z(t) \rangle$ for a state in the bulk is shown in Fig. 6 for the case of $J_x = 0, J_y = 0.1, J_z = 0.5$. The simulation was converged at a time-step of $\Delta t = 0.375$ and a memory length of $L = 3$. The forward-backward propagator MPO was compressed using singular value decomposition with a relative error cutoff of 10^{-10} to obtain an MPO with a maximum bond dimension of $w_p^{\max} = 46$ and an average bond dimension of $\bar{w}_p = 30$. While we report the dynamics of the bulk spin here, the edge spin has previously been studied [34]. Our simulations reproduces the previously obtained results for the edge spin.

IV. CONCLUSION

System-solvent decomposition is used in various fields of study and is simulated using the Feynman-Vernon influence functional. In such applications there is a neces-

sity to have quite a small dimensional quantum system for computational feasibility. However, many interesting problems involve extended systems that can be modeled as collection of very small dimensional units. Typical examples are cases that involve spin-chains to model magnetism and charge or exciton transfers.

Recently various methods based on tensor networks have been proposed to compress the path integrals, thereby reducing the storage requirements for the simulation. This tensor network path integral methods naturally suggest a further decomposition along the system dimension leading to a multisite method. In this paper, we have introduced such a multisite tensor network method called MS-TNPI. The structure of this MS-TNPI method is a 2D extension of the 1D MPS structure used in the AP-TNPI [28] or the time-evolving matrix product operators method [24].

The most essential part of MS-TNPI method starts with a definition of a forward-backward propagator for the extended system. This is a common problem that is dealt with in the tDMRG, TDVP and TEBD literature. We show how we can essentially use these propagators and refactorize them to obtain the current 2D structure. We also discuss how by viewing the tensor network as a collection of rows containing the path amplitude tensor corresponding to every site, it becomes possible to now apply the influence functional MPO for the local bath in a systematic manner. Exploration of the behavior of existing methods for MPO-MPS style wave function propagation in the current context would be an interesting avenue of research. Especially methods like W^{I,II} and TDVP, if adapted to the current framework, would enable the simulation of significantly long-ranged interacting systems in presence of local phononic modes.

A salient feature of this method is that it can generate the full reduced density tensor corresponding to the entire extended system at any point of time. While having this global knowledge means that the storage requirements increase with the number of sites, we show that the presence of the local vibrational bath helps decrease the growth of the bond dimension of the reduced density tensor MPS. An added advantage of this feature is that it enables us to do memory iteration corresponding to the finiteness of the non-Markovian memory quite trivially.

MS-TNPI is demonstrated through illustrative examples of various spin-chains coupled to local harmonic baths. We simulate the Ising model, the XXZ-model and the Heisenberg model with various different parameters. The method is extremely efficient for all the parameters tested. There are interesting features of the dynamics for the various phases of the XXZ-model that require further investigation. This would be the subject of future work.

MS-TNPI promises to be an exciting method for extended systems. It makes it possible to study various energy and charge transfer processes, and loss of coherence in chains of qubits. Such applications shall be the focus of our research in the near future. The novelty of the structure opens up possibilities for further improve-

ments and developments of which we have only begun scratching the surface.

ACKNOWLEDGMENTS

A.B. acknowledges the support of the Computational Chemical Center: Chemistry in Solution and at Interfaces funded by the US Department of Energy under Award No. DE-SC0019394. P.W. acknowledges the Miller Institute for Basic Research in Science for funding.

Appendix A: System Forward-Backward Propagator in MPO representation

For the simple case of nearest-neighbor interacting Hamiltonian, it is very easy to define an algorithm for calculating the second-order Suzuki-Trotter split forward-backward propagator. This is a “forward-backward” version of the second-order time-evolved block decimation scheme [6].

Let the Hamiltonian be factorized as:

$$\hat{H}_0 = \sum_{j=1}^{P-1} \hat{\mathcal{H}}_{j,(j+1)} \quad (A1)$$

where $\hat{\mathcal{H}}_{j,(j+1)}$ takes the one-body term into account as well. To get the second-order splitting, it is usual to incorporate the terminal single body terms fully into the corresponding terms. Everything else is split in halves:

$$\hat{\mathcal{H}}_{1,2} = \hat{h}_1^{(1)} + \hat{h}_{1,2}^{(2)} + \frac{1}{2}\hat{h}_2^{(1)} \quad (A2)$$

$$\hat{\mathcal{H}}_{j,(j+1)} = \frac{1}{2}\hat{h}_j^{(1)} + \hat{h}_{j,(j+1)}^{(2)} + \frac{1}{2}\hat{h}_{(j+1)}^{(1)}, \quad 2 \leq j < N-1 \quad (A3)$$

$$\hat{\mathcal{H}}_{(P-1),P} = \frac{1}{2}\hat{h}_{(P-1)}^{(1)} + \hat{h}_{(P-1),P}^{(2)} + \hat{h}_P^{(1)}. \quad (A4)$$

Now, the terms are grouped as “even” and “odd” as follows:

$$\hat{\mathcal{H}}_{\text{odd}} = \sum_{\substack{j \text{ odd} \\ 1 \leq j < P}} \hat{\mathcal{H}}_{j,(j+1)} \quad (A5)$$

$$\hat{\mathcal{H}}_{\text{even}} = \sum_{\substack{j \text{ even} \\ 1 \leq j < P}} \hat{\mathcal{H}}_{j,(j+1)}. \quad (A6)$$

First, we define the two-body propagators, and separate out the system sites using a singular value decomposition:

$$\begin{aligned} U(s_{j,0}^+, s_{(j+1),0}^+, s_{j,1}^+, s_{(j+1),1}^+ \Delta t) \\ = \langle s_{j,1}^+, s_{(j+1),1}^+ | \exp \left(-\frac{i}{\hbar} \hat{\mathcal{H}}_{j,(j+1)} \Delta t \right) | s_{j,0}^+, s_{(j+1),0}^+ \rangle \\ = \sum_{\alpha_j} B_{s_{j,0}^+, s_{j,1}^+, \alpha_j} B_{\alpha_j, s_{(j+1),0}^+, s_{(j+1),1}^+} \end{aligned} \quad (A7)$$

The forward-backward propagators corresponding to the even and odd parts can be formed simply by taking the direct product of the forward and backward propagator matrix elements. We just discuss the odd part for brevity:

$$K_{\text{odd}}(S_0^\pm, S_1^\pm, \Delta t) = \prod_{\substack{j \text{ odd} \\ 1 \leq j < P}}^j U(s_{j,0}^+, s_{(j+1),0}^+, s_{j,1}^+, s_{(j+1),1}^+ \Delta t) \\ \times U^\dagger(s_{j,0}^-, s_{(j+1),0}^-, s_{j,1}^-, s_{(j+1),1}^- \Delta t) \quad (\text{A8})$$

The odd and even propagators can now be used to generate the full single time-step forward-backward propagator under a second order Suzuki-Trotter factorization:

$$K(S_0^\pm, S_1^\pm, \Delta t) = \sum_{\kappa, \lambda} K_{\text{odd}}(S_0^\pm, \kappa, \frac{1}{2}\Delta t) \\ \times K_{\text{even}}(\kappa, \lambda, \Delta t) \\ \times K_{\text{odd}}(\lambda, S_1^\pm, \frac{1}{2}\Delta t). \quad (\text{A9})$$

It is simple to recast Eq. (A9) into an MPO using Eq. (A7) leading to Eq. (8).

[1] S. R. White, Density matrix formulation for quantum renormalization groups, *Phys. Rev. Lett.* **69**, 2863 (1992).

[2] U. Schollwöck, The density-matrix renormalization group, *Rev. Mod. Phys.* **77**, 259 (2005).

[3] U. Schollwöck, The density-matrix renormalization group: A short introduction, *Philos. Trans. A Math. Phys. Eng. Sci.* **369**, 2643 (2011).

[4] U. Schollwöck, The density-matrix renormalization group in the age of matrix product states, *Ann. Phys. (N. Y.)* **326**, 96 (2011).

[5] S. R. White and A. E. Feiguin, Real-Time Evolution Using the Density Matrix Renormalization Group, *Phys. Rev. Lett.* **93**, 10.1103/physrevlett.93.076401 (2004).

[6] S. Paeckel, T. Köhler, A. Swoboda, S. R. Manmana, U. Schollwöck, and C. Hubig, Time-evolution methods for matrix-product states, *Ann. Phys. (N. Y.)* **411**, 167998 (2019).

[7] X. Xie, Y. Liu, Y. Yao, U. Schollwöck, C. Liu, and H. Ma, Time-dependent density matrix renormalization group quantum dynamics for realistic chemical systems, *J. Chem. Phys.* **151**, 224101 (2019).

[8] Y. Tanimura, Numerically “exact” approach to open quantum dynamics: The hierarchical equations of motion (HEOM), *J. Chem. Phys.* **153**, 020901 (2020).

[9] R. P. Feynman and F. L. Vernon, The theory of a general quantum system interacting with a linear dissipative system, *Ann. Phys. (N. Y.)* **24**, 118 (1963).

[10] Y. Tanimura and R. Kubo, Time Evolution of a Quantum System in Contact with a Nearly Gaussian-Markoffian Noise Bath, *J. Phys. Soc. Jpn.* **58**, 101 (1989).

[11] C. Duan, Q. Wang, Z. Tang, and J. Wu, The study of an extended hierarchy equation of motion in the spin-boson model: The cutoff function of the sub-Ohmic spectral density, *J. Chem. Phys.* **147**, 164112 (2017).

[12] T. Ikeda and G. D. Scholes, Generalization of the hierarchical equations of motion theory for efficient calculations with arbitrary correlation functions, *J. Chem. Phys.* **152**, 204101 (2020).

[13] B. Popescu, H. Rahman, and U. Kleinekathöfer, Chebyshev Expansion Applied to Dissipative Quantum Systems, *J. Phys. Chem. A* **120**, 3270 (2016).

[14] T. Banerjee and N. Makri, Quantum-Classical Path Integral with Self-Consistent Solvent-Driven Reference Propagators, *J. Phys. Chem. B* **117**, 13357 (2013).

[15] R. Lambert and N. Makri, Quantum-classical path integral. I. Classical memory and weak quantum nonlocality, *J. Chem. Phys.* **137**, 22A552 (2012).

[16] R. Lambert and N. Makri, Quantum-classical path integral. II. Numerical methodology, *J. Chem. Phys.* **137**, 22A553 (2012).

[17] P. L. Walters and N. Makri, Quantum-Classical Path Integral Simulation of Ferrocene–Ferrocenium Charge Transfer in Liquid Hexane, *J. Phys. Chem. Lett.* **6**, 4959 (2015).

[18] P. L. Walters and N. Makri, Iterative quantum-classical path integral with dynamically consistent state hopping, *J. Chem. Phys.* **144**, 044108 (2016).

[19] N. Makri and D. E. Makarov, Tensor propagator for iterative quantum time evolution of reduced density matrices. I. Theory, *J. Chem. Phys.* **102**, 4600 (1995).

[20] N. Makri and D. E. Makarov, Tensor propagator for iterative quantum time evolution of reduced density matrices. II. Numerical methodology, *J. Chem. Phys.* **102**, 4611 (1995).

[21] N. Makri, Blip decomposition of the path integral: Exponential acceleration of real-time calculations on quantum dissipative systems, *J. Chem. Phys.* **141**, 134117 (2014).

[22] N. Makri, Blip-summed quantum-classical path integral with cumulative quantum memory, *Faraday Discuss.* **195**, 81 (2016).

[23] N. Makri, Iterative blip-summed path integral for quantum dynamics in strongly dissipative environments, *J. Chem. Phys.* **146**, 134101 (2017).

[24] A. Strathearn, P. Kirton, D. Kilda, J. Keeling, and B. W. Lovett, Efficient non-Markovian quantum dynamics using time-evolving matrix product operators, *Nat. Commun* **9**, 10.1038/s41467-018-05617-3 (2018).

[25] M. R. Jørgensen and F. A. Pollock, Exploiting the Causal Tensor Network Structure of Quantum Processes to Efficiently Simulate Non-Markovian Path Integrals, *Phys. Rev. Lett.* **123**, 10.1103/physrevlett.123.240602 (2019).

[26] D. Gribben, A. Strathearn, J. Iles-Smith, D. Kilda, A. Nazir, B. W. Lovett, and P. Kirton, Exact quantum dynamics in structured environments, *Phys. Rev. Res.* **2**, 10.1103/physrevresearch.2.013265 (2020).

[27] E. Ye and G. K.-L. Chan, Constructing tensor network influence functionals for general quantum dynamics, *J. Chem. Phys.* **155**, 044104 (2021).

[28] A. Bose and P. L. Walters, A tensor network representation of path integrals: Implementation and analysis,

arXiv pre-print server (2021).

[29] A. Bose, A Pairwise Connected Tensor Network Representation of Path Integrals, arXiv pre-print server (2021).

[30] J. Ren, Z. Shuai, and G. Kin-Lic Chan, Time-Dependent Density Matrix Renormalization Group Algorithms for Nearly Exact Absorption and Fluorescence Spectra of Molecular Aggregates at Both Zero and Finite Temperature, *J. Chem. Theory Comput.* **14**, 5027 (2018).

[31] N. Makri, Communication: Modular path integral: Quantum dynamics via sequential necklace linking, *J. Chem. Phys.* **148**, 101101 (2018).

[32] N. Makri, Modular path integral methodology for real-time quantum dynamics, *J. Chem. Phys.* **149**, 214108 (2018).

[33] S. Kundu and N. Makri, Modular path integral for discrete systems with non-diagonal couplings, *J. Chem. Phys.* **151**, 074110 (2019).

[34] S. Kundu and N. Makri, Modular path integral for finite-temperature dynamics of extended systems with intramolecular vibrations, *J. Chem. Phys.* **153**, 044124 (2020).

[35] A. Lerose, M. Sonner, and D. A. Abanin, Influence Matrix Approach to Many-Body Floquet Dynamics, *Phys. Rev. X* **11**, 10.1103/physrevx.11.021040 (2021).

[36] M. Fishman, S. R. White, and E. M. Stoudenmire, The ITensor Software Library for Tensor Network Calculations, arXiv pre-print server (2020).

[37] A. O. Caldeira and A. J. Leggett, Path integral approach to quantum Brownian motion, *Physica A: Statistical Mechanics and its Applications* **121**, 587 (1983).

[38] N. Makri, The Linear Response Approximation and Its Lowest Order Corrections: An Influence Functional Approach, *J. Phys. Chem. B* **103**, 2823 (1999).

[39] J. Haegeman, J. I. Cirac, T. J. Osborne, I. Pižorn, H. Verschelde, and F. Verstraete, Time-Dependent Variational Principle for Quantum Lattices, *Phys. Rev. Lett.* **107**, 070601 (2011).

[40] R. Orús, A practical introduction to tensor networks: Matrix product states and projected entangled pair states, *Ann. Phys. (N. Y.)* **349**, 117 (2014).

[41] M. Yang and S. R. White, Time-dependent variational principle with ancillary Krylov subspace, *Phys. Rev. B* **102**, 094315 (2020).

[42] A. J. Daley, C. Kollath, U. Schollwöck, and G. Vidal, Time-dependent density-matrix renormalization-group using adaptive effective Hilbert spaces, *J. Stat. Mech. Theory Exp.* **2004**, P04005 (2004).

[43] G. Vidal, Efficient Simulation of One-Dimensional Quantum Many-Body Systems, *Phys. Rev. Lett.* **93**, 040502 (7).

[44] M. P. Zaletel, R. S. K. Mong, C. Karrasch, J. E. Moore, and F. Pollmann, Time-evolving a matrix product state with long-ranged interactions, *Phys. Rev. B* **91**, 165112 (4).

[45] N. Makri, Small matrix modular path integral: Iterative quantum dynamics in space and time, *Phys. Chem. Chem. Phys.* **23**, 12537 (2021).

[46] M. V. Rakov and M. Weyrauch, Spin- $\frac{1}{2}$ XXZ Heisenberg chain in a longitudinal magnetic field, *Phys. Rev. B* **100**, 134434 (10).